Electronic Supplementary Information

Si regulation of hydrogen adsorption on nanoporous PdSi hybrids towards enhancing electrochemical hydrogen evolution activity

Zhandong Ren,[a,1,*] *Hucheng Jiang*,[a,1] *Min Yuan*,[a] *Zhiqiang Xie*,[a] *Li Deng*,[a] *Juanjuan Han*,[a] *Kangjie Lyu*,[b] *Yuchan Zhu*,[a,*] *Li Xiao*[b] *and Lin Zhuang*[b]

[a] School of Chemical and Environmental Engineering, Wuhan Polytechnic University, Wuhan, 430023, P. R. China.

[b] College of Chemistry and Molecular Sciences, Hubei Key Lab of Electrochemical Power Sources, Wuhan University, Wuhan, 430072, PR China.

[1] Z. D. Ren and H. C. Jiang contributed equally to this work.

* Corresponding author:

Zhandong Ren, Professor, School of Chemical and Environmental Engineering, Wuhan Polytechnic University, Wuhan, 430023, P. R. China. E-mail: renzhandong@163.com. Tel.: 86-27-83943956.

Yuchan Zhu, Professor, School of Chemical and Environmental Engineering, Wuhan Polytechnic University, Wuhan, 430023, P. R. China. E-mail: zhuyuchan@163.com. Tel.: 86-27-83943956.

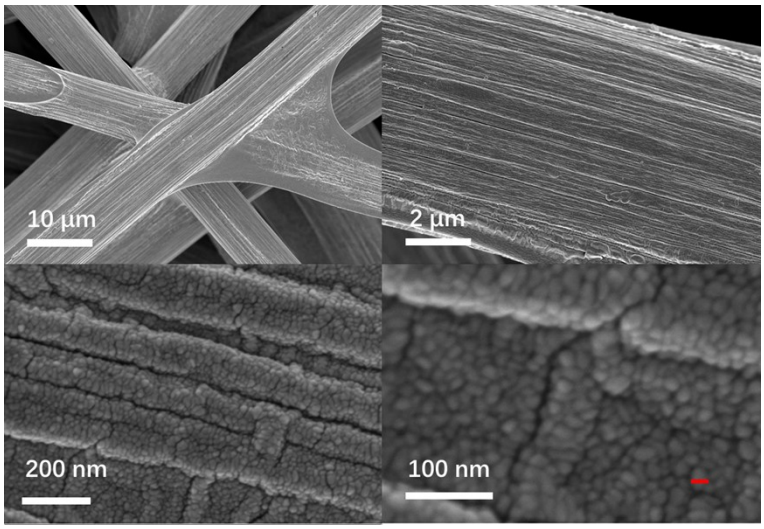

Figure S1 SEM images of Pd. (The red scale represents 20 nm.)

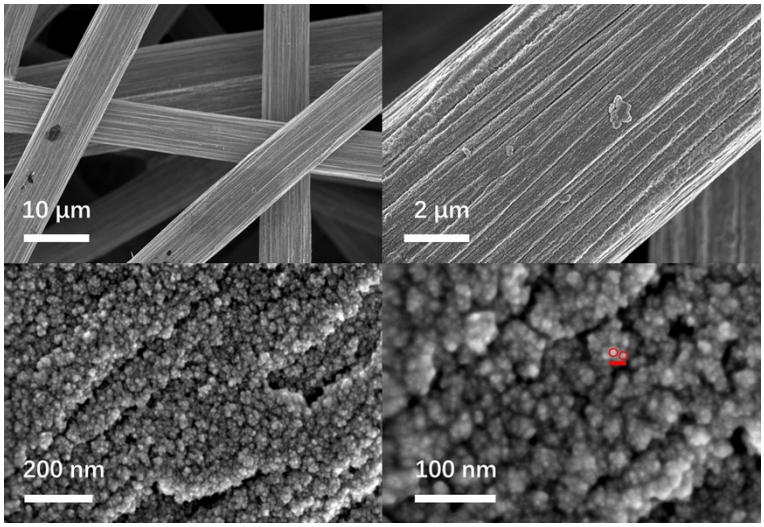

Figure S2 SEM images of $Pd_{15}Si$. (The red scale represents 20 nm.)

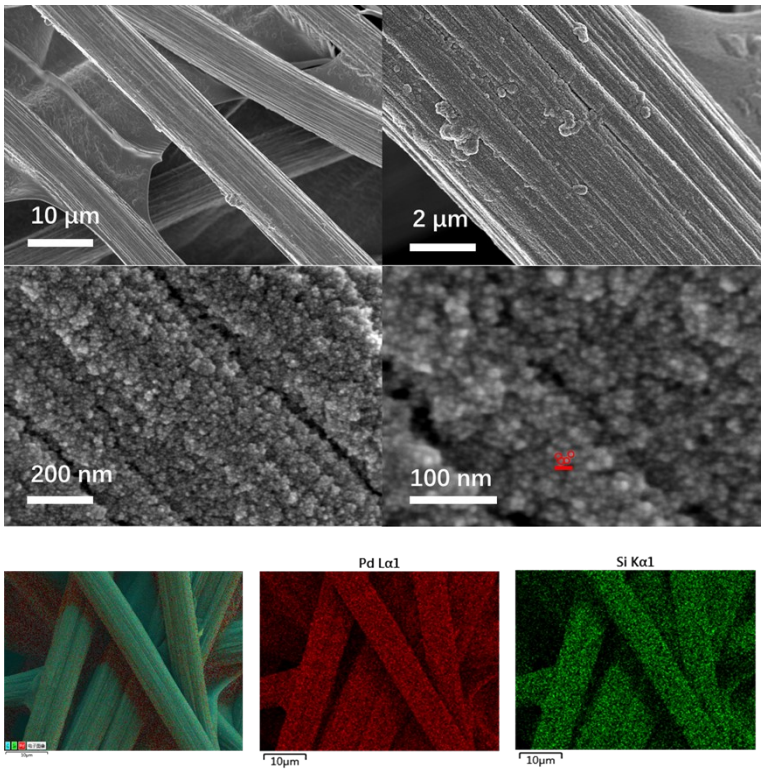

Figure S3 SEM and mapping images of Pd_3Si. (The red scale represents 20 nm.)

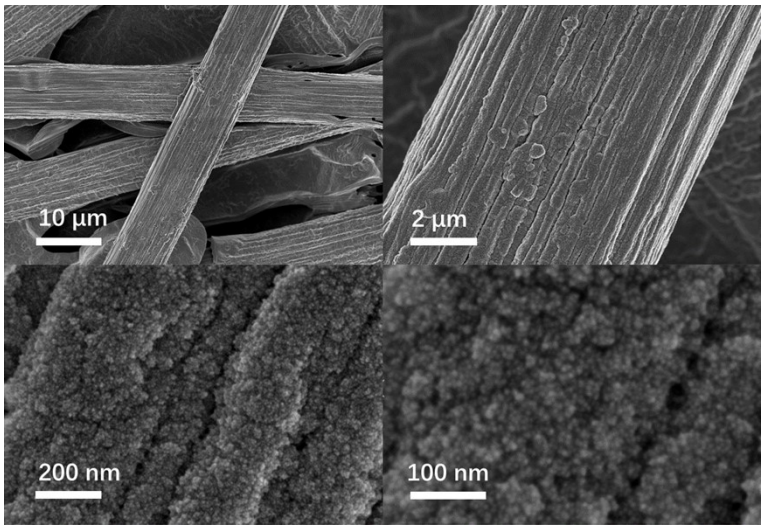

Figure S4 SEM images of $Pd_{2.5}Si$.

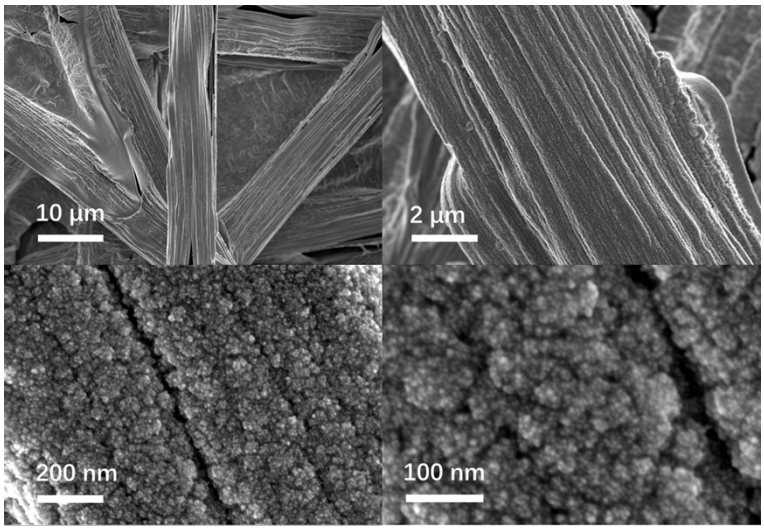

Figure S5 SEM images of Pd_2Si.

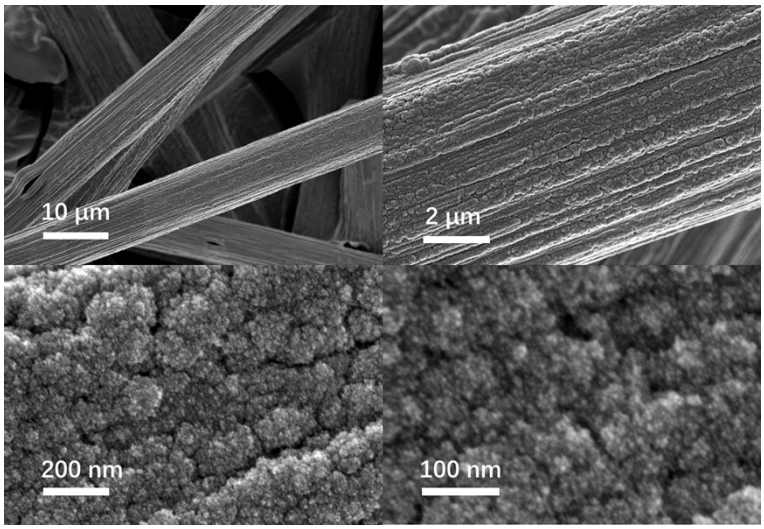

Figure S6 SEM images of $Pd_{1.5}Si$.

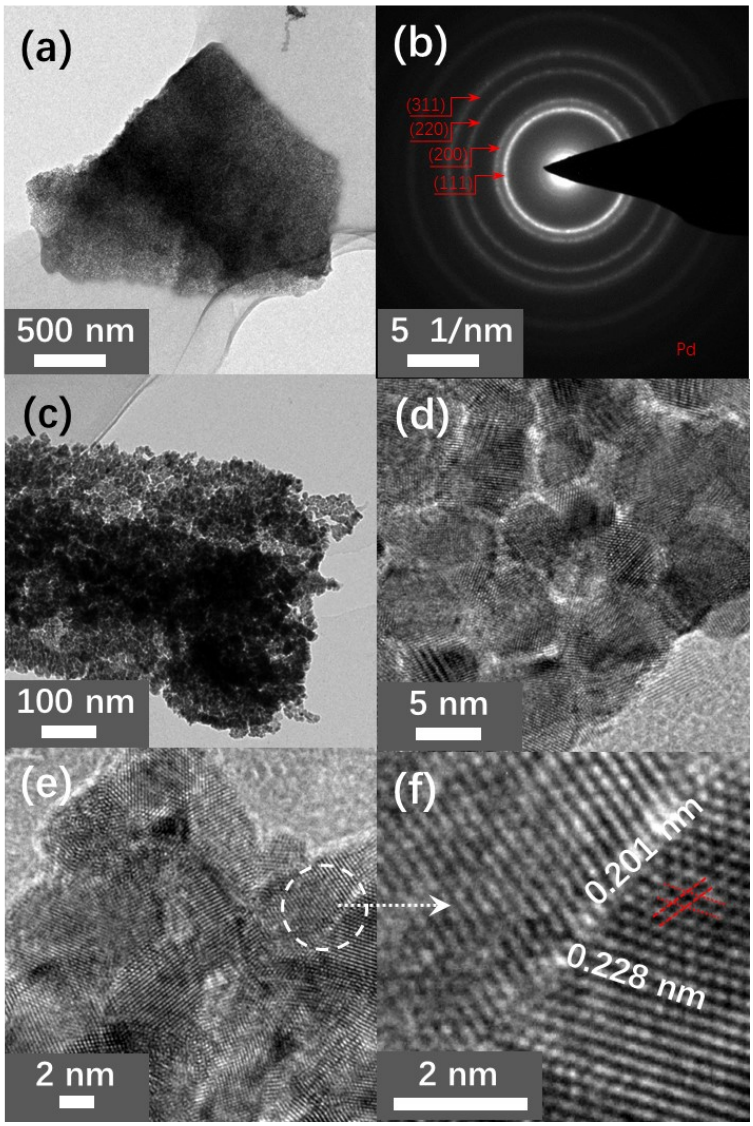

Figure S7 TEM and HRTEM images of Pd.

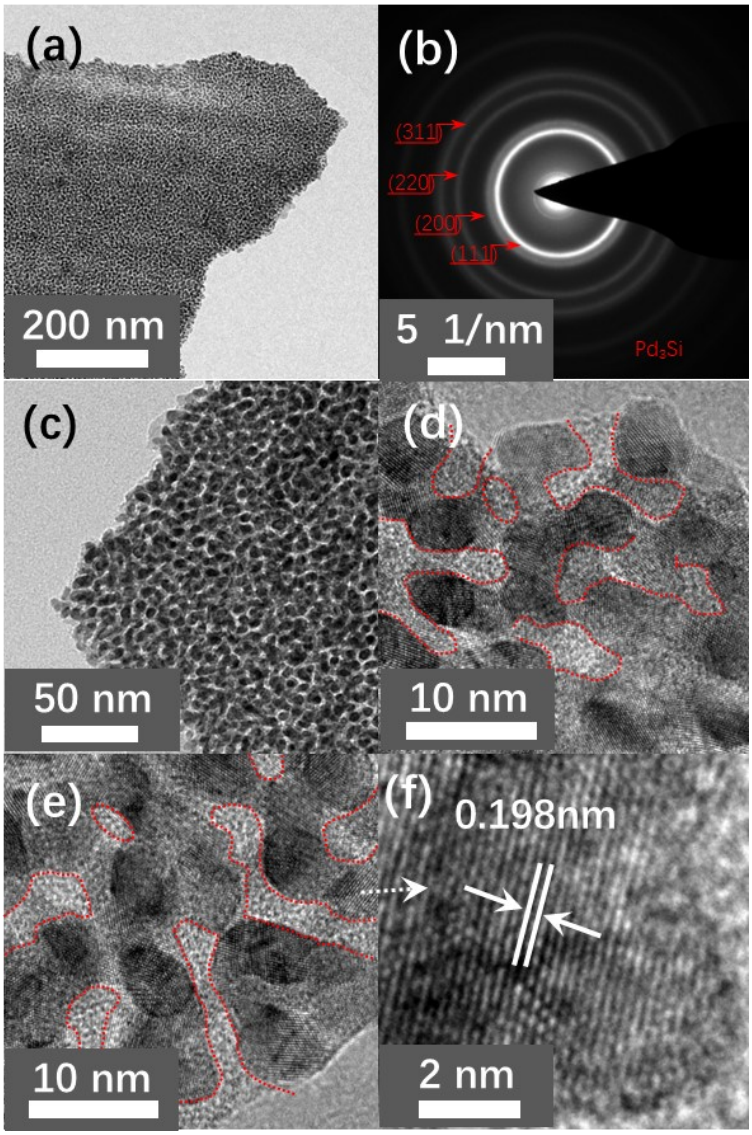

Figure S8 TEM and HRTEM images of Pd_3Si.

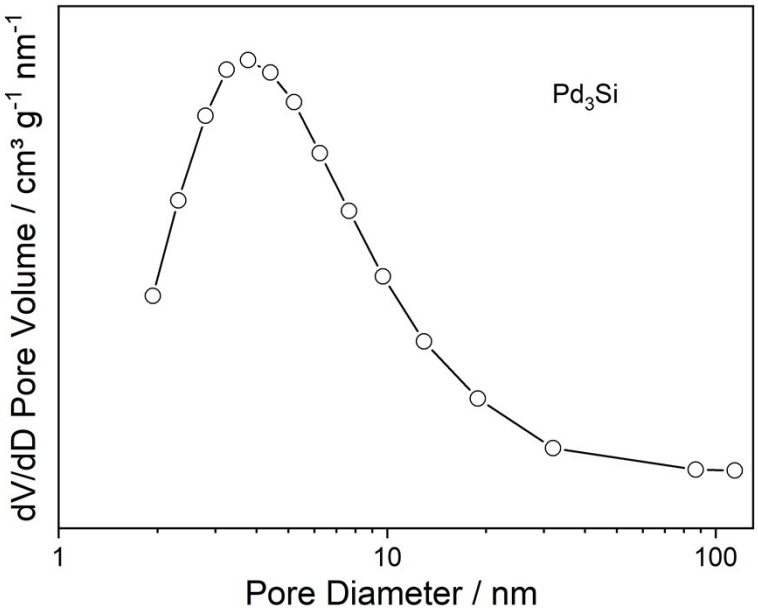

Figure S9 Pore size distributions of Pd_3Si.

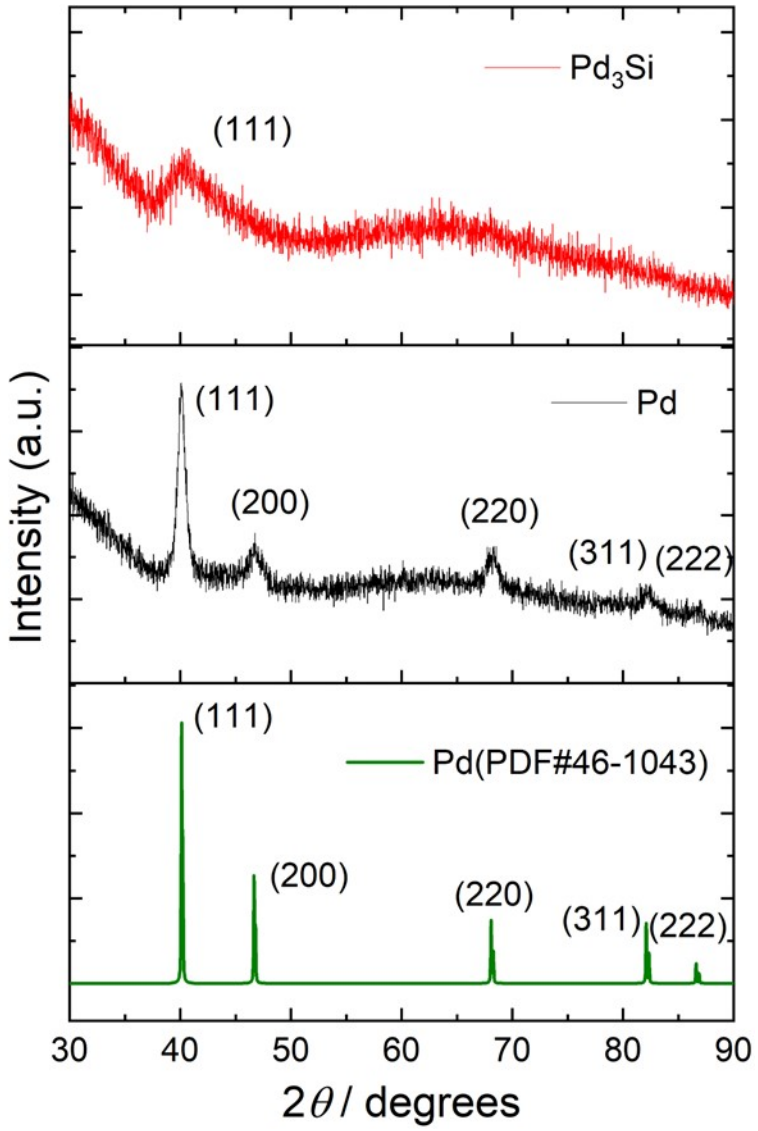

Figure S10 X-ray diffraction patterns of Pd and Pd_3Si.

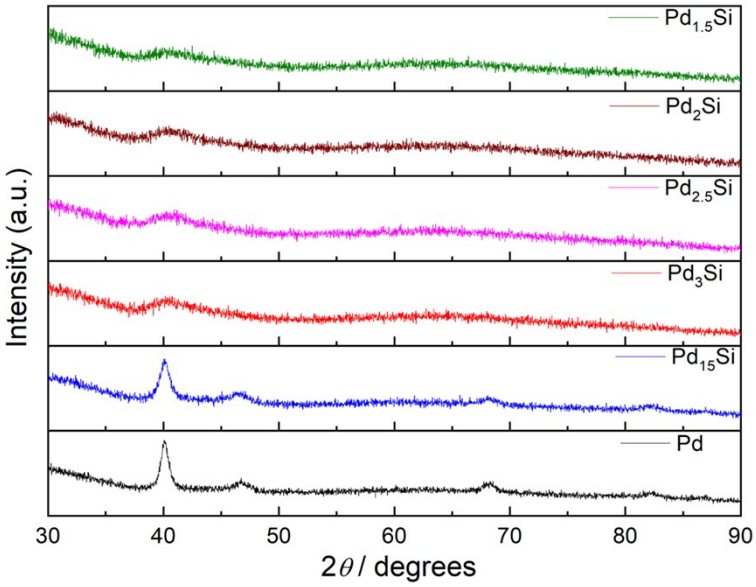

Figure S11 X-ray diffraction patterns of NP-PdSi hybrids with different ratios.

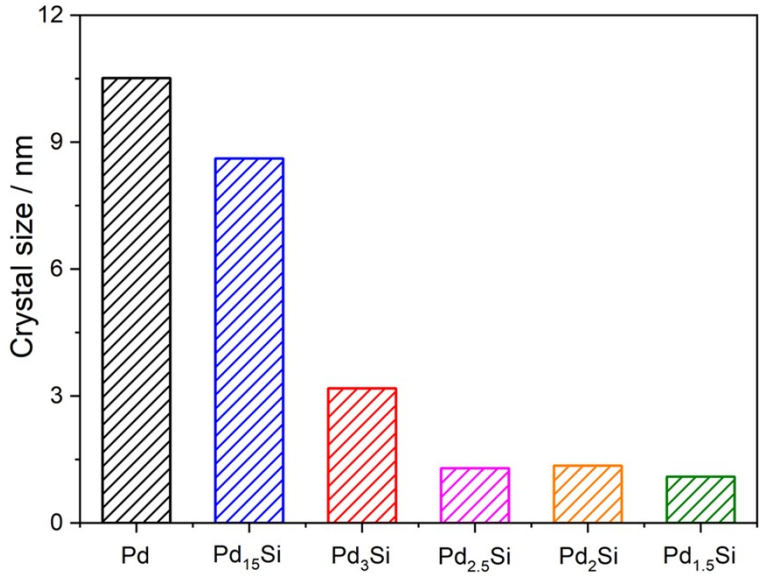

Figure S12 The grain sizes of NP-PdSi hybrids with different ratios.

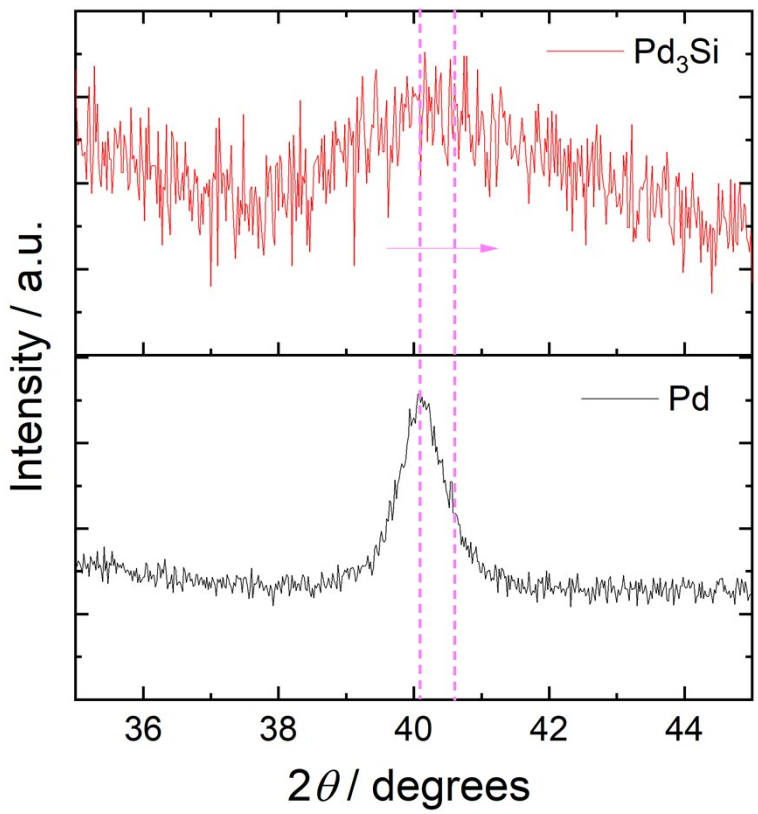

Figure S13 X-ray diffraction patterns of Pd and Pd_3Si in range of 35 ~ 45°.

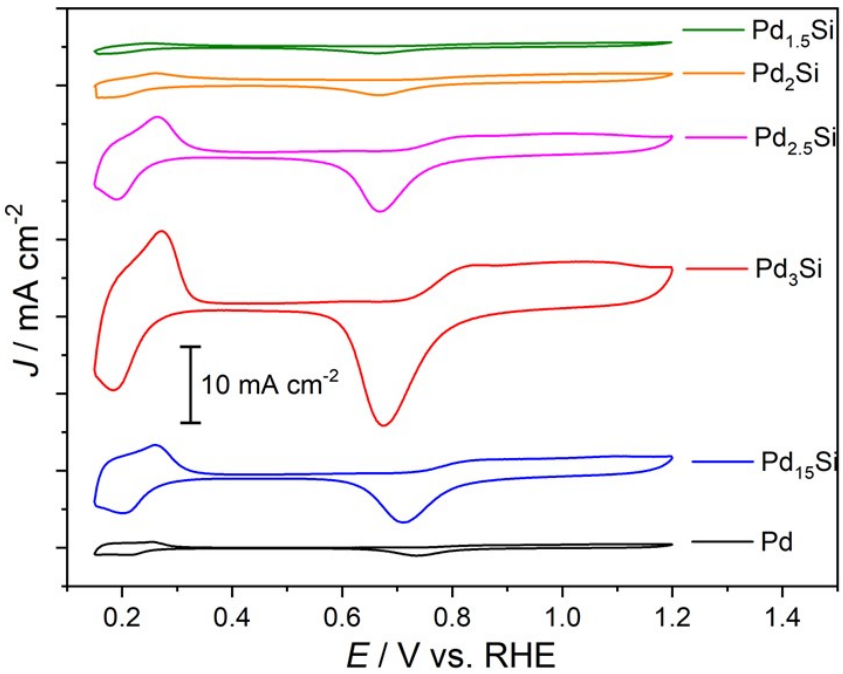

Figure S14 Cyclic voltammetry curves of Pd and NP-PdSi hybrids with different proportions.

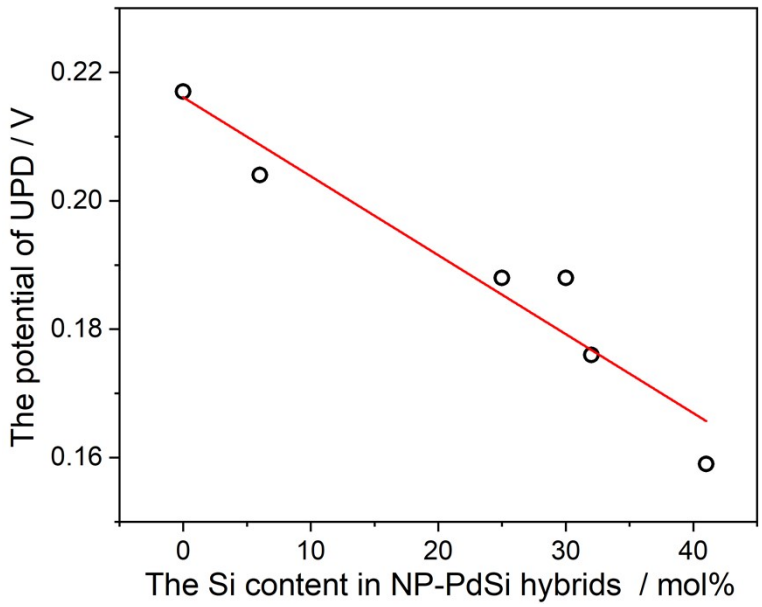

Figure S15 The effect of Si content on UPD potential of NP-PdSi hybrids with different ratios.

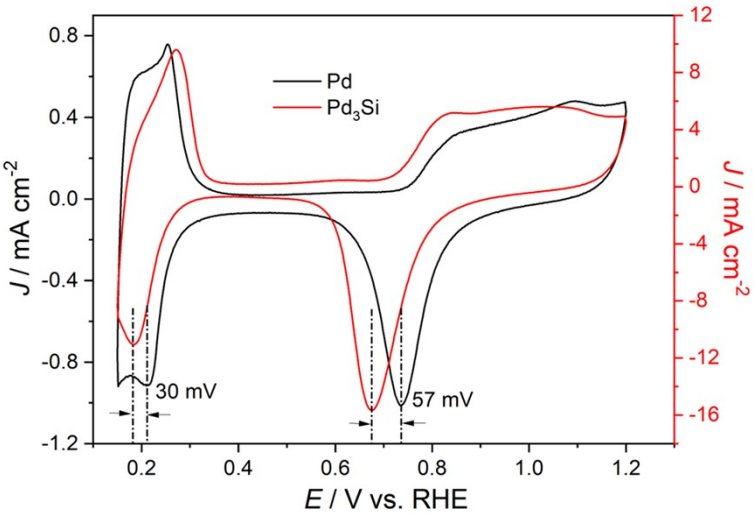

Figure S16 Cyclic voltammetry curves of Pd and Pd_3Si.

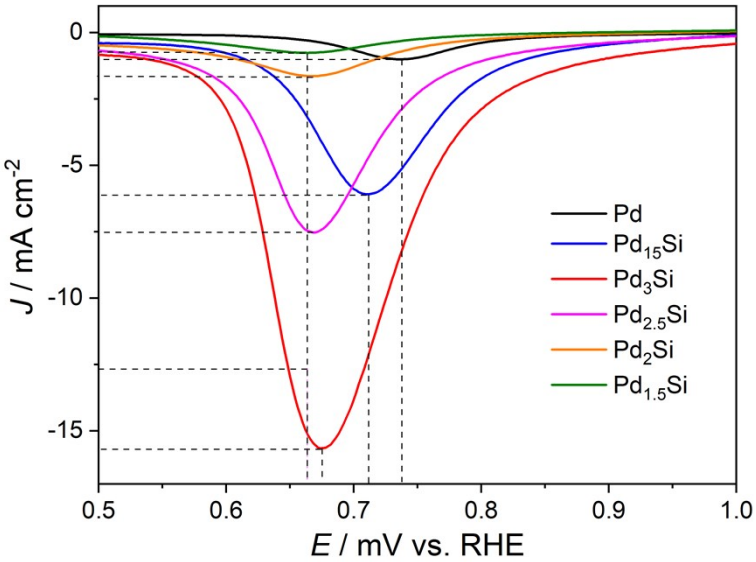

Figure S17 The reduction peaks of OH_{ads} of NP-PdSi hybrids with different ratios.

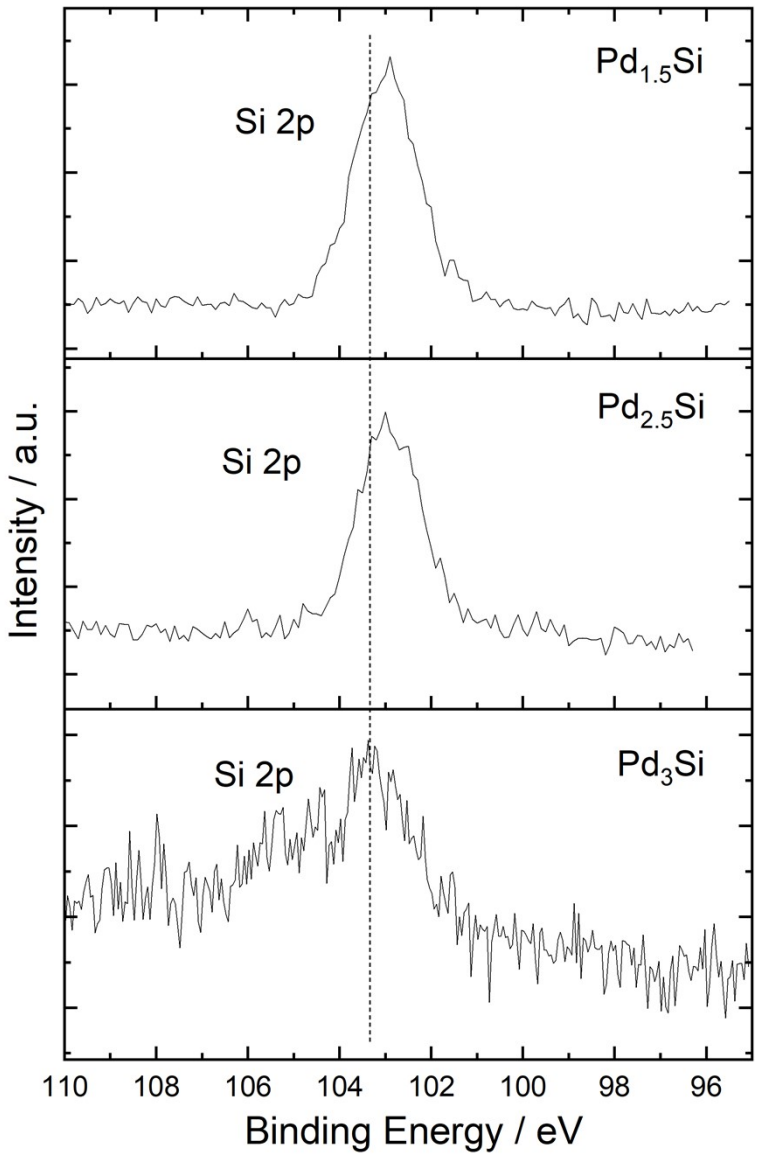

Figure S18 The XPS core-level spectra of Si 2p obtained from $Pd_{1.5}Si$ (a), $Pd_{2.5}Si$ (b) and Pd_3Si (c).

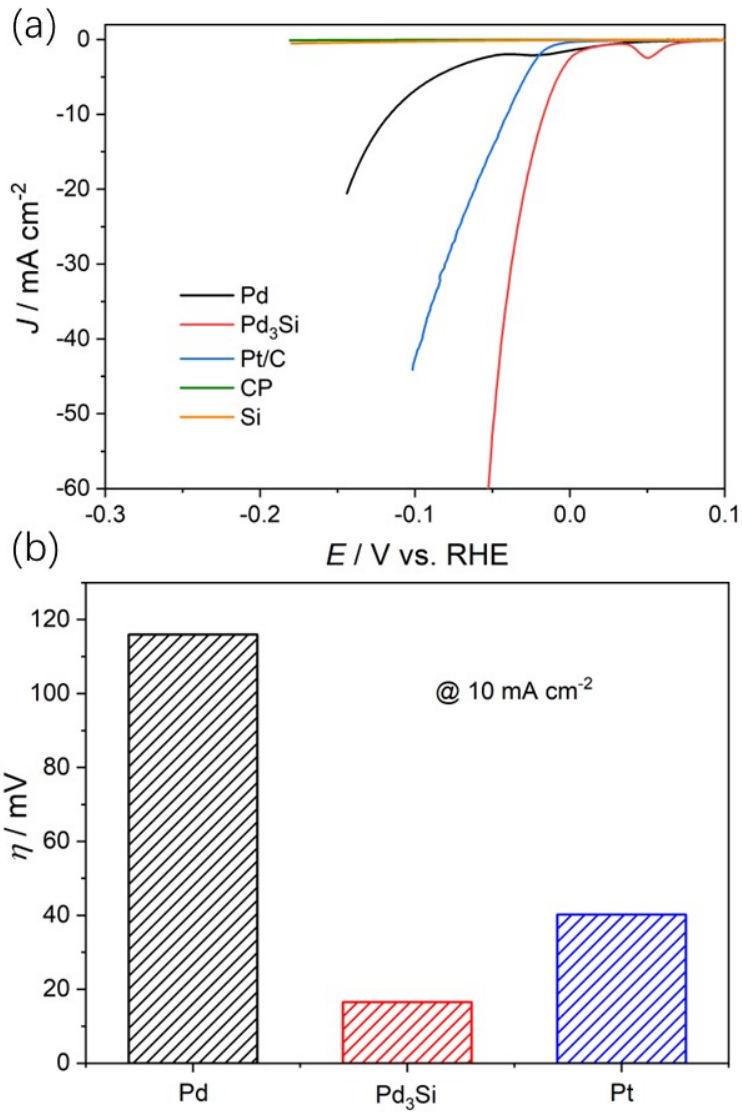

Figure S19 The hydrogen evolution activities of Pd, Pd_3Si, Pt/C, CP and Si (a). The η_{10} values of Pd, Pd_3Si and Pt/C (b).

For carbon paper (CP) and Si, there are no obvious HER activities in the investigated potential range.

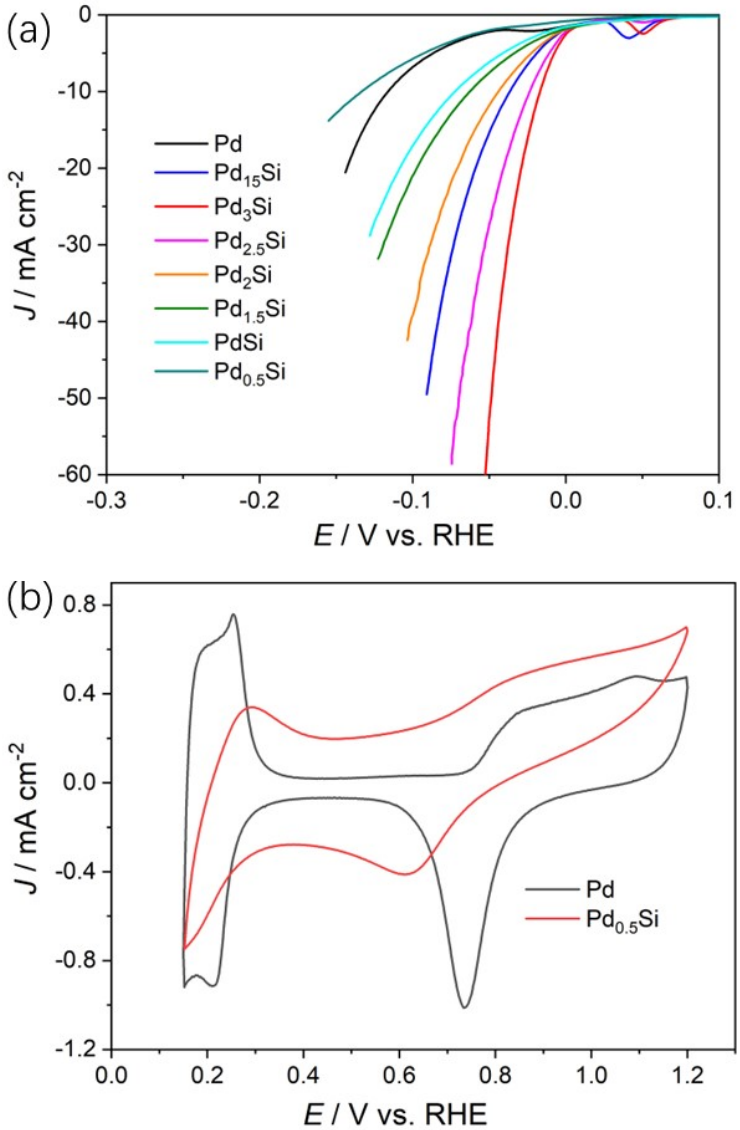

Figure S20 The hydrogen evolution activities of Pd and NP-PdSi hybrids (a). Cyclic voltammetry curves of Pd and Pd_3Si (b).

When the content of Si in NP-PdSi hybrids is further increased, and the ratio of Pd to Si reaches 1:1 and 0.5:1, their HER activities are further reduced. The HER activity of $Pd_{0.5}Si$ is lower than that of Pd. This is because the excessive content of Si on the electrode surface reduces the exposure of Pd atoms. It can be confirmed from CV diagram that the ECSA of $Pd_{0.5}Si$ is obviously lower than that of Pd. Furthermore, in the CV of $Pd_{0.5}Si$, the electrochemical characteristics originally belonging to Pd have become very inconspicuous.

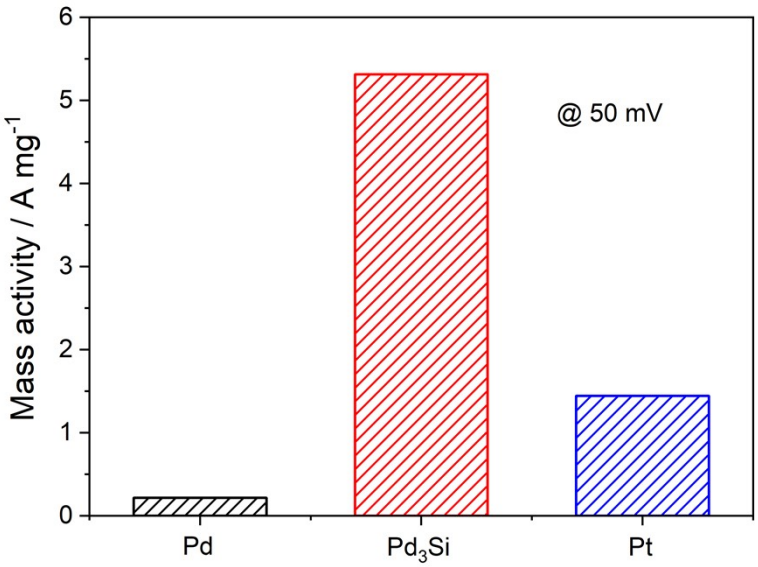

Figure S21 The MA activities of of Pd, Pd_3Si and Pt/C.

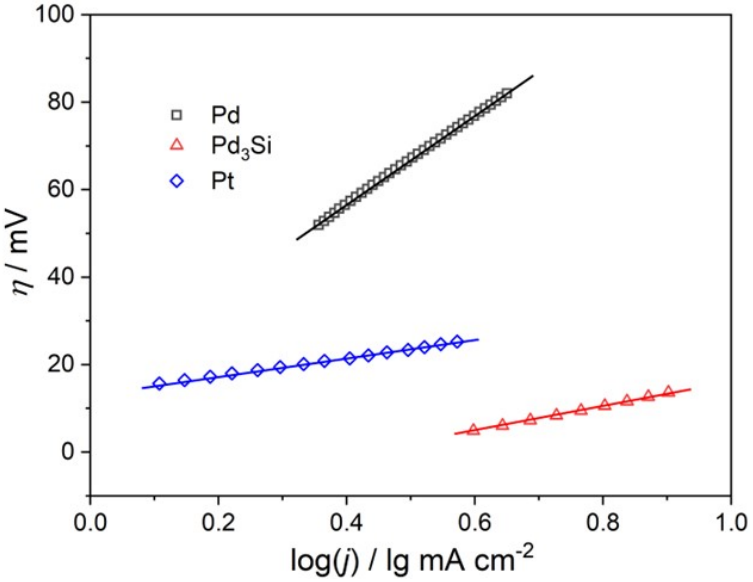

Figure S22 The Tafel curves of of Pd, Pd_3Si and Pt/C.

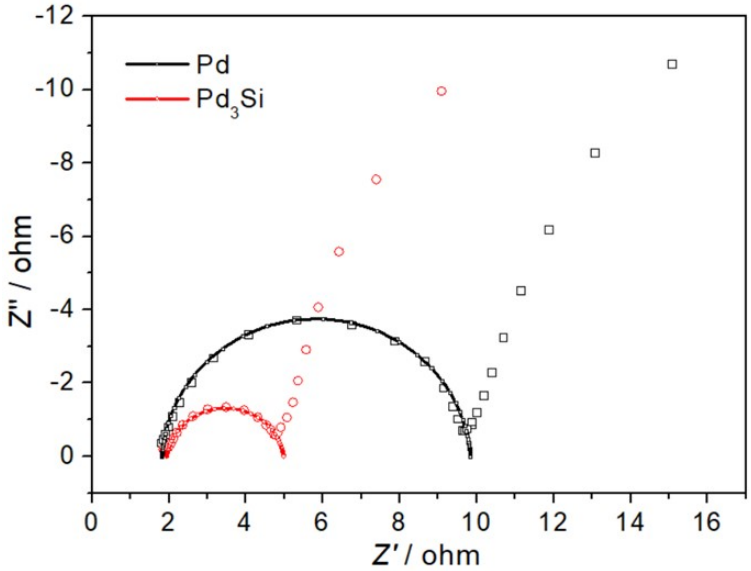

Figure S23 The electrochemical impedance spectroscopy (EIS) of Pd and Pd_3Si.

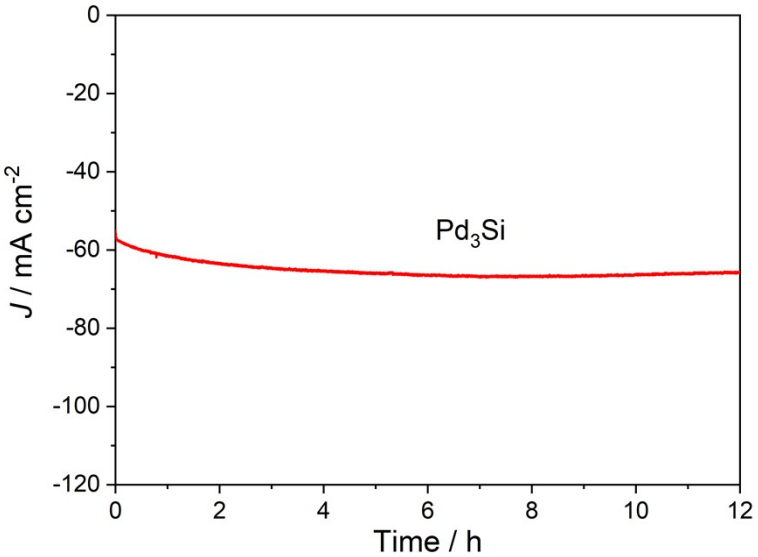

Figure S24 The long-term stability test of Pd_3Si.

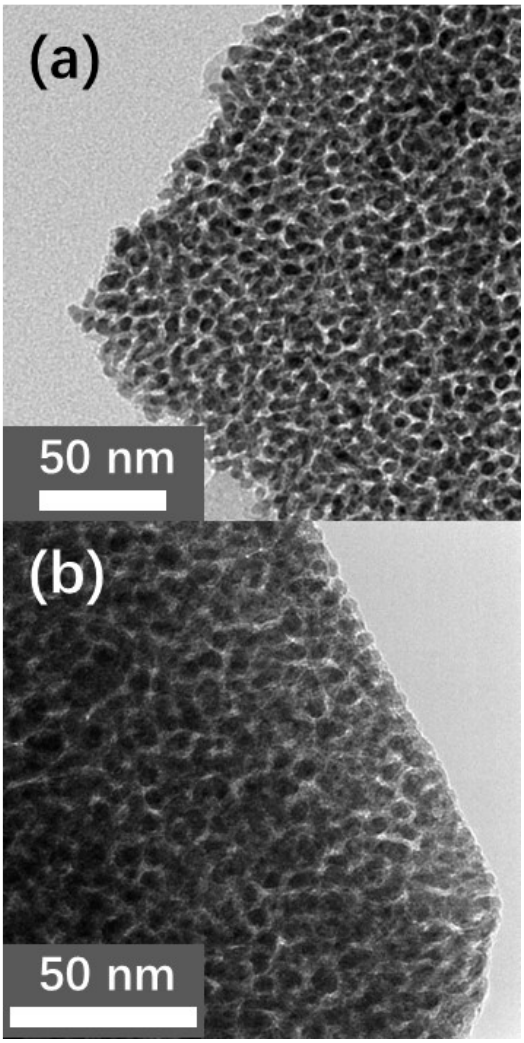

Figure S25 TEM images of Pd_3Si before (a) and after (b) the long-term stability test.

Table S1 Composition analysis of NP-PdSi hybrids with different sputtering power by X-ray fluorescence

Catalyst	Sputtering power / W		Content / mol%		Pd loading
	Pd	Si	Pd	Si	/μg cm^{-2}
$Pd_{15}Si$[a]	30	40	94.18	5.82	10
Pd_3Si[a]	30	80	74.97	25.03	10
$Pd_{2.5}Si$[a]	30	100	70.14	29.86	10
Pd_2Si[a]	30	120	67.96	32.04	10
$Pd_{1.5}Si$[a]	30	150	59.00	41.00	10
$Pd_{1.0}Si$[a]	30	240	47.53	52.47	10
$Pd_{0.5}Si$[b]	15	240	31.26	68.74	10
Pd_3Si after 10h stability test	---	---	73.76	26.24	---

[a] Sputtering time is 10 min. [b] Sputtering time is 20 min.

Table S2. Comparison of HER activities between optimized NP-PdSi hybrids and other Pd-based electrocatalysts in literatures.

Catalyst	**Electrolyte**	**η_{10} (mV)**	**Tafel slope mV dec^{-1}**	**References**
Pd_3Si	**0.5 M H_2SO_4**	**16.5**	**27.7**	**This work**
$PdCu_{0.2}H_{0.43}$	0.5 M H_2SO_4	28	23	Nano Lett. 2022, 22, 1391−1397. **(1)**
N-PdIr bimetallene	0.5 M H_2SO_4	26	30.3	J. Mater. Chem. A, 2022, 10, 8364–8370.
	1.0 M KOH	34	81.9	**(2)**
Pd,Re-MoS_2	0.5 M H_2SO_4	46	72	Adv. Energy Mater. 2022, 12, 2103823. **(3)**
PdSNC	0.5 M H_2SO_4	30	56.7	ACS Appl. Energy Mater. 2021, 4, 575−585. **(4)**
Pd_4S-SNC	0.5 M H_2SO_4	32	52	Small 2021, 17, 2007511. **(5)**
Pd_2B@PEI mNPs	0.5 M H_2SO_4	15	44	J. Mater. Chem. A, 2021,9, 21123-21131. **(6)**
GO-Pd_6P	0.5 M H_2SO_4	133	60	Dalton Trans., 2022, 51, 6537–6542. **(7)**
Nanoporous Pd-Ag-Al	0.5 M H_2SO_4	11	26	ACS Energy Lett. 2019, 4, 1379−1386. **(8)**
	1.0 M KOH	16	56	
Porous Pd@Ru	0.5 M H_2SO_4	37	33	ACS Appl. Mater. Interfaces 2018, 10,
	1.0 M KOH	30	30	34147−34152. **(9)**
$Pd_{83.5}Ir_{16.5}$	0.5 M H_2SO_4	73	43.6	Inorg. Chem. 2020, 59, 5, 3321–3329. **(10)**
Pd/Bi/Cu HNAs	0.5 M H_2SO_4	79	61	ACS Appl. Mater. Interfaces 2019, 11, 6248−6256. **(11)**
heterophase Pd_{45}@Ir_{55}	0.1M $HClO_4$	11	26	Adv. Mater. 2021, 2107399. **(12)**
CuPd/Pd	0.5 M H_2SO_4	10	34	Adv. Funct. Mater. 2021, 2100883. **(13)**
Pd NPs-Bis-24h	0.5 M H_2SO_4	59.6	30.0	Adv. Mater. 2020, 1902964. **(14)**
GDY-Pd1	0.5 M H_2SO_4	201 (η_{500})	27	Adv. Funct. Mater., 2022, 32, 2111501. **(15)**
Pd@G-NSs	0.5 M H_2SO_4	32	33	ACS Appl. Mater. Interfaces 2020, 12, 15500−15506. **(16)**
2H-VS_2-Pd	0.5 M H_2SO_4	157 (η_{20})	75	Inorg. Chem. 2020, 59, 14, 10197–10207. **(17)**
$NiCo_2S_4$/Pd	0.5 M H_2SO_4	87	70	ACS Appl. Mater. Interfaces 2018, 10,
	1.0 M KOH	83	123	22248−22256. **(18)**
$[Pd(BTA)\text{-}rGO]_{red}$	0.5 M H_2SO_4	127	55	ACS Appl. Energy Mater. 2019, 2, 11, 8098–8106. **(19)**
0.75 Pd/Mo_3N_2	0.5 M H_2SO_4	45	88	Phys. Chem. Chem. Phys., 2022, 24, 771-
	1.0 M KOH	65	70	777. **(20)**
Pd/TiO2	0.1M $HClO_4$	63(η_{20})	36	ACS Appl. Mater. Interfaces 2020, 12, 24,
	0.1 M KOH	284(η_{20})	99	27037–27044. **(21)**
PdNP@GNF	0.1M $HClO_4$	220	141	ChemSusChem 2021, 14, 4973 –4984. **(22)**
Pd@MoO_3	0.5 M H_2SO_4	71	42.8	ACS Appl. Mater. Interfaces 2019, 11, 31, 27798–27804. **(23)**

(1) Jia Y.; Huang T.-H.; Lin S.; Guo L.; Yu Y.-M.; Wang J.-H.; Wang K.-W.; Dai S. Stable Pd−Cu Hydride Catalyst for Efficient Hydrogen Evolution. *Nano Lett.* **2022**, *22*, 1391−1397.

(2) Mao Q.; Deng K.; Wang W.; Wang P.; Xu Y.; Wang Z.; Li X.; Wang L.; Wang H. N-doping induced lattice-strained porous PdIr bimetallene for pH-universal hydrogen evolution electrocatalysis. *J. Mater. Chem. A* **2022**, *10*, 8364–8370.

(3) Luo Z.; Li J.; Li Y.; Wu D.; Zhang L.; Ren X.; He C.; Zhang Q.; Gu M.; Sun X. Band Engineering Induced Conducting 2H-Phase MoS_2 by Pd-S-Re Sites Modification for Hydrogen Evolution Reaction. *Adv. Energy Mater.* **2022**, *12*, 2103823.

(4) Naveen M. H.; Huang Y.; Kantharajappa S. B.; Seo K.-D.; Park D.-S.; Shim Y.-B. Enhanced Electrocatalytic Activities of In Situ Produced Pd/S/N-Doped Carbon in Oxygen Reduction and Hydrogen Evolution Reactions. *ACS Appl. Energy Mater.* **2021**, *4*, 575−585.

(5) Huang Y.; Seo K.-D.; Park D.-S.; Park H.; Shim Y.-B. Hydrogen Evolution and Oxygen Reduction Reactions in Acidic Media Catalyzed by Pd_4S Decorated N/S Doped Carbon Derived from Pd Coordination Polymer. *Small* **2021**, *17*, 2007511.

(6) Xu Y.; Liu M.; Ren T.; Wang S.; Liu T.; Wang Z.; Li X.; Wang L.; Wang H. Regulation of the surface micro-structure and crystal phase of Pd_2B mesoporous nanoparticles for enhanced hydrogen evolution electrocatalysis. *J. Mater. Chem. A* **2021**, *9*, 21123-21131.

(7) Oswal P.; Sood K.; Singh S.; Arora A.; Bahuguna A.; Purohit S.; Kumar A. Single source precursor route for the first graphene oxide–Pd_6P nanocomposite: application in electrochemical hydrogen evolution reaction. *Dalton Trans.* **2022**, *51*, 6537–6542.

(8) Yao R.-Q.; Zhou Y.-T.; Shi H.; Zhang Q.-H.; Gu L.; Wen Z.; Lang X.-Y.; Jiang Q. Nanoporous Palladium−Silver Surface Alloys as Efficient and pH-Universal Catalysts for the Hydrogen Evolution Reaction. *ACS Energy Lett.* **2019**, *4*, 1379−1386.

(9) Luo Y.; Luo X.; Wu G.; Li Z.; Wang G.; Jiang B.; Hu Y.; Chao T.; Ju H.; Zhu J.; Zhuang Z.; Wu Y.; Hong X.; Li Y. Mesoporous Pd@Ru Core−Shell Nanorods for Hydrogen Evolution Reaction in Alkaline Solution. *ACS Appl. Mater. Interfaces* **2018**, *10*, 34147−34152.

(10) Wang C.; Xu H.; Shang H.; Jin L.; Chen C.; Wang Y.; Yuan M.; Du Y. Ir-Doped Pd Nanosheet Assemblies as Bifunctional Electrocatalysts for Advanced Hydrogen Evolution Reaction and Liquid Fuel Electrocatalysis. *Inorg. Chem.* **2020**, *59*, 3321–3329.

(11) Zheng L.; Zheng S.; Wei H.; Du L.; Zhu Z.; Chen J.; Yang D. Palladium/Bismuth/Copper Hierarchical Nano-Architectures for Efficient Hydrogen Evolution and Stable Hydrogen Detection. *ACS Appl. Mater. Interfaces* **2019**, *11*, 6248−6256.

(12) Ge Y.; Wang X.; Chen B.; Huang Z.; Shi Z.; Huang B.; Liu J.; Wang G.; Chen Y.; Li L.; Lu S.; Luo Q.; Yun Q.; Zhang H. Preparation of fcc-2H-fcc Heterophase Pd@Ir Nanostructures for High-Performance Electrochemical Hydrogen Evolution. *Adv. Mater.* **2021**, *34*, 2107399.

(13) Xie H.; Chen S.; Liang J.; Wang T.; Hou Z.; Wang H.-L.; Chai G.; Li Q. Weakening Intermediate Bindings on CuPd/Pd Core/shell Nanoparticles to Achieve Pt-Like Bifunctional Activity for Hydrogen Evolution and Oxygen Reduction Reactions. *Adv. Funct. Mater.* **2021**, *31*, 2100883.

(14) Cheng H.; Yang N.; Liu G.; Ge Y.; Huang J.; Yun Q.; Du Y.; Sun C.-J.; Chen B.; Liu J.; Zhang H. Ligand-Exchange-Induced Amorphization of Pd Nanomaterials for Highly Efficient Electrocatalytic Hydrogen Evolution Reaction. *Adv. Mater.* **2020**, *32*, 1902964.

(15) Zhang D.; Zheng X.; Qi L.; Xue Y.; He F.; Li Y. Controlled Growth of Single-Crystal Pd Quantum Dots on 2D Carbon for Large Current Density Hydrogen Evolution. *Adv. Funct. Mater.* **2022**, *32*, 2111501.

(16) Nguyen V.-T.; Ha H.; Nguyen N.-A.; An H.; Kim H. Y.; Choi H.-S. *In Situ* Engineering of Pd Nanosponge Armored with Graphene Dots Using Br^- toward High-Performance and Stable Electrocatalyst for the Hydrogen Evolution Reaction. *ACS Appl. Mater. Interfaces* **2020**, *12*, 15500−15506.

(17) Karthick K.; Bijoy T. K.; Sivakumaran A.; Basha A. B. M.; Murugan P.; Kundu S. Enhancing Hydrogen Evolution Reaction Activities of 2H-Phase VS_2 Layers with Palladium Nanoparticles. *Inorg. Chem.* **2020**, *59*, 10197–10207.

(18) Sheng G.; Chen J.; Li Y.; Ye H.; Hu Z.; Fu X.-Z.; Sun R.; Huang W.; Wong C.-P. Flowerlike $NiCo_2S_4$ Hollow Sub-Microspheres with Mesoporous Nanoshells Support Pd Nanoparticles for Enhanced Hydrogen Evolution Reaction Electrocatalysis in Both Acidic and Alkaline Conditions. *ACS Appl. Mater. Interfaces* **2018**, *10*, 22248−22256.

(19) Alex C.; Bhat S. A.; John N. S.; Yelamaggad C. V. Highly Efficient and Sustained Electrochemical Hydrogen Evolution by Embedded Pd-Nanoparticles on a Coordination Polymer-Reduced Graphene Oxide Composite. *ACS Appl. Energy Mater.* **2019**, *2*, 8098–8106.

(20) Raheem S. A.; Shen H.; Thomas T.; Yang M. Integrating trace amounts of Pd nanoparticles into Mo_3N_2 nanobelts for an improved hydrogen evolution reaction. *Phys. Chem. Chem. Phys.* **2022**, *24*, 771-777.

(21) Chalgin A.; Chen W.; Xiang Q.; Wu Y.; Li F.; Shi F.; Song C.; Tao P.; Shang W.; Wu J. Manipulation of Electron Transfer between Pd and TiO_2 for Improved Electrocatalytic Hydrogen Evolution Reaction Performance. *ACS Appl. Mater. Interfaces* **2020**, *12*, 27037–27044.

(22) Aygün M.; Guillen-Soler M.; Vila-Fungueiriño J. M.; Kurtoglu A.; Chamberlain T. W.; Khlobystov A. N.; Gimenez-Lopez M. C. Palladium Nanoparticles Hardwired in Carbon Nanoreactors Enable Continually Increasing Electrocatalytic Activity During the Hydrogen Evolution Reaction. *ChemSusChem* **2021**, *14*, 4973 – 4984.

(23) Li J.; Cheng Y.; Zhang J.; Fu J.; Yan W.; Xu Q. Confining Pd Nanoparticles and Atomically Dispersed Pd into Defective MoO_3 Nanosheet for Enhancing Electro- and Photocatalytic Hydrogen Evolution Performances. *ACS Appl. Mater. Interfaces* **2019**, *11*, 27798–27804.

Table S3. Tafel slopes and exchange current densities of NP-PdSi hybrids and Pt/C with the noble metal loading of 10 μg cm^{-2}.

Catalyst	Tafel slope ($mV\ dec^{-1}$)	Exchange current density (j_0) ($mA\ cm^{-2}$)
Pd	101.4	0.69
$Pd_{15}Si$	49.1	2.03
Pd_3Si	27.7	2.71
$Pd_{2.5}Si$	38.9	2.60
Pd_2Si	59.3	2.06
$Pd_{1.5}Si$	82.6	1.94
Pt/C	20.3	0.77